Analysis of Anisotropic Graphene Platelet Heat Spreaders to Reduce Hot Spot Temperature and Temperature Non-Uniformity

Sohail R. Reddy and George S. Dulikravich
Department of Mechanical and Materials Engineering, MAIDROC Laboratory
Florida International University
10555 West Flagler Street, Miami, Florida 33174, USA
Telephone: +1 954 554 0368 Email: {sredd001; dulikrav}@fiu.edu Web page: http://maidroc.fiu.edu

ABSTRACT

This work investigates the effect of thin film graphene heat spreaders on the maximum temperature of integrated electric circuits. An electronic chip with a 4 x 3mm footprint featured a centrally located 0.5 x 0.5mm hot spot located on the top wall. The remainder of the top wall was exposed to a uniform background heat flux. The graphene heat spreaders were applied to the top wall of an optimized cooling array of micro pin-fins having airfoil cross-sections. A fully 3D conjugate heat transfer analysis was performed to investigate the effects of different heat spreader thicknesses on the temperature of the hot spot and the temperature distribution on the hot surface. Both isotropic and anisotropic thermal conductivities of heat spreaders were considered. The conjugate heat transfer analysis also incorporated thermal contact resistance.

KEY WORDS: thermal management, graphene nano-platelets, electronic cooling, convection, pin-fin array, heat spreaders

NOMENCLATURE

C_p	thermal capacity per unit mass (J kg^{-1} K^{-1})
t	thickness (m)
k	thermal conductivity (W m^{-1} K^{-1})
p	pressure (N m^{-2})
T	temperature (K)
t	thickness (μm)
V	fluid velocity (m s^{-1})

Greek symbols

μ	kinematic viscosity (m^2 s^{-1})
ρ	mass density (kg m^{-3})

INTRODUCTION

Civilian, and especially military, applications of the new generation of micro-electronic chips are expected to reach heat flux levels of at least 500 W cm^{-2} at the background and significantly in excess of 1000 W cm^{-2} at the hot spots [1]. Soaring temperatures at these hot spots pose a major challenge to the thermal management community, because they limit the processor speed.

Often, forced cooling methods alone are not effective in lowering the temperature spike at the hot spot. One approach to remedy this problem is to have the hot surface coated with thin film heat spreaders to lower the hot spot temperature spike and make hot surface temperature more uniform. Fukutani and Shakouri [2] investigated analytically Si and SiGe thin film micro-cooler and concluded that the hot spot temperature can be decreased by up to 30ºC. Wang *et al.* [3] studied the effectiveness of thin film heat spreaders in conjunction with a micro-channel cooling configuration. Mayer and Ram [4] performed optimization of heat sinks coated with thin films. Smalc *et al.* [5] investigated the use of natural graphite as heat spreaders with much higher thermal conductivity. Reddy *et al.* [6] presented comparative analyses of isotropic graphene thin film and diamond thin film heat spreader performances.

Graphene nano-platelets (GNPs) are a viable alternative to most thin film materials not only because they are less expensive than diamond, but also because they possess a much higher directional thermal conductivity. The extremely high and anisotropic thermal conductivity makes them an ideal choice in dissipating thermal energy away from the hot spot resulting in lower temperature and higher temperature uniformity. The effect of graphene heat spreaders on maximum temperature have previously been numerically investigated by Reddy *et al.* [6], Barua *et al.* [7], Bae *et al.* [8] and Subrina *et al.* [9]. Their work however assumed that the thermal conductivity is an isotropic property, which is not always the case. All numerical methods also ignored contact resistance between the thin films and the base substrate material.

This work investigates the effect of GNP coating applied to an optimized array of micro pin-fins cooled by forced convection. Unlike previous computational work, the GNP thin films considered here feature anisotropic thermal conductivity. The thermal contact resistance is also incorporated into the computational model. The micro pin-fin geometry used in this work is defined in the same manner as presented by Reddy *et al.* [10,11] and is shown in Fig. 1, where the blue surface represents the coating applied to the top surface. The effect of thin film thickness and type of GNP on maximum temperature and temperature distribution is investigated.

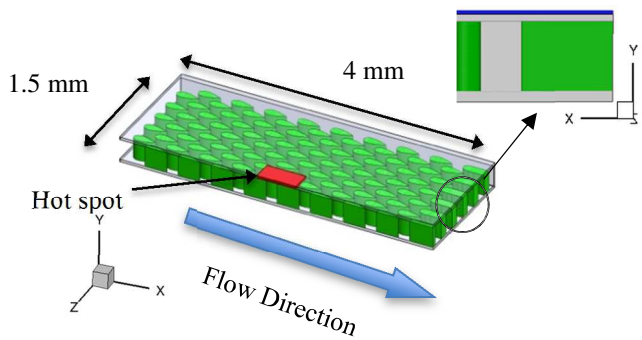

Figure 1. One half of a micro pin-fin cooling array and geometric dimensions as considered in this study

CONJUGATE HEAT TRANSFER ANALYSIS

The thermal boundary conditions, hydrodynamic boundary conditions and geometric configurations, shown in Table 1, were arrived at using the inverse design approach proposed by Reddy and Dulikravich [11] and were kept constant throughout the analysis. The entire top surface was exposed to a uniform background heat flux. A significantly higher heat flux was enforced at the small, centrally located hot spot. All other external surfaces were thermally insulated, ensuring all of the heat is removed by the cooling water. The outlet was pressurized at 20kPa and the inlet water temperature was 30°C.

Table 1. Geometric parameters and boundary conditions used for each analysis

Pin-fin cross section	Airfoil
Pin-fin chord length (μm)	280
Pin-fin thickness (μm)	120
Pin-fin height (μm)	250
Coolant inlet speed (m s^{-1})	5.5
Background heat flux (W cm^{-2})	875
Hot spot heat flux (W cm^{-2})	2200

A computational grid of approximately eight million cells was used for each conjugate heat transfer analysis. A comparison of the results obtained using a grid of 11 million elements showed that the results deviated by less than 1% thereby assuring grid convergence. Five layers of structured grid were placed on each solid-fluid interface. The incompressible Reynolds Averaged Navier-Stokes (RANS) equations were solved for the fluid domain. The continuity, momentum and energy equations are given as

$$\nabla \bullet \vec{V} = 0 \tag{1}$$

$$\rho\left(\vec{V} \bullet \nabla\right)\vec{V} = \nabla \bullet \left[-p\underline{I} + \mu\left(\nabla\vec{V} + \left(\nabla\vec{V}\right)^{T}\right)\right] \tag{2}$$

$$\rho C_p\left(\vec{V} \bullet \nabla\right)T = \left(\vec{V} \bullet \nabla\right)p + \nabla \bullet \left(k\nabla T\right) \tag{3}$$

The heat transfer was assumed to obey Fourier's Law and be diffusive in the graphene layers since the size of the graphene layers is much larger than the phonon mean free path [12-14]. The steady-state heat conduction equation with spatially varying thermal conductivity was solved in the solid domain. This model was previously validated against analytical solutions [15].

$$\nabla \cdot \left(k\nabla T\right) = 0 \tag{4}$$

Alfieri *et al.* [16] showed that even for Reynolds numbers between 80-180, as in this work, significant vortex shedding occurs at the micro pin-fins. The standard k-ε turbulence model was used to simulate the low Re turbulent flow in all cases.

The influence of each thin film heat spreader coating on temperature uniformity is considered using the Coefficient of Variation (CV) defined as

$$CV = \frac{\sigma}{T_{ave}} \tag{5}$$

where

$$\sigma = \sqrt{\frac{1}{N}\sum_{i=1}^{N}\left(T_i - T_{ave}\right)^2} \tag{6}$$

and

$$T_{ave} = \frac{1}{N}\sum_{i=1}^{N} T_i \tag{7}$$

where N is the number of computational grid cells. For comparison purposes the micro pin-fin array configuration was analyzed without the heat spreader under the boundary conditions specified in Table 1.

Table 2 shows the maximum temperature and the coefficient of variation for the micro pin-fin array configuration without any heat spreader.

Table 2. Maximum temperature and CV for configuration without thin film heat spreader coating

Maximum temperature (K)	346.76
Coefficient of variation	0.01173

Because there was no constraint placed on the overall height of the chip + thin films, for verification of accuracy purpose, cases were also considered where the top wall of the IC was coated with various thicknesses of silicon. Results shown in Table 3 confirm the high accuracy of the temperature field analysis.

Table 3. Maximum temperature and CV for configurations with different thin film coating thicknesses made of Silicon

t (μm)	Max. Temp. (K)	$CV_{Hotspot}$	$CV_{Background}$	ΔT_{avg}
10	348.83	0.00982	0.00950	16.199
15	348.88	0.00970	0.00935	16.168
20	347.16	0.00920	0.00933	15.242
25	347.28	0.00903	0.00922	15.293

Figure 2 shows the temperature distribution on the top surface of each of the four configurations.

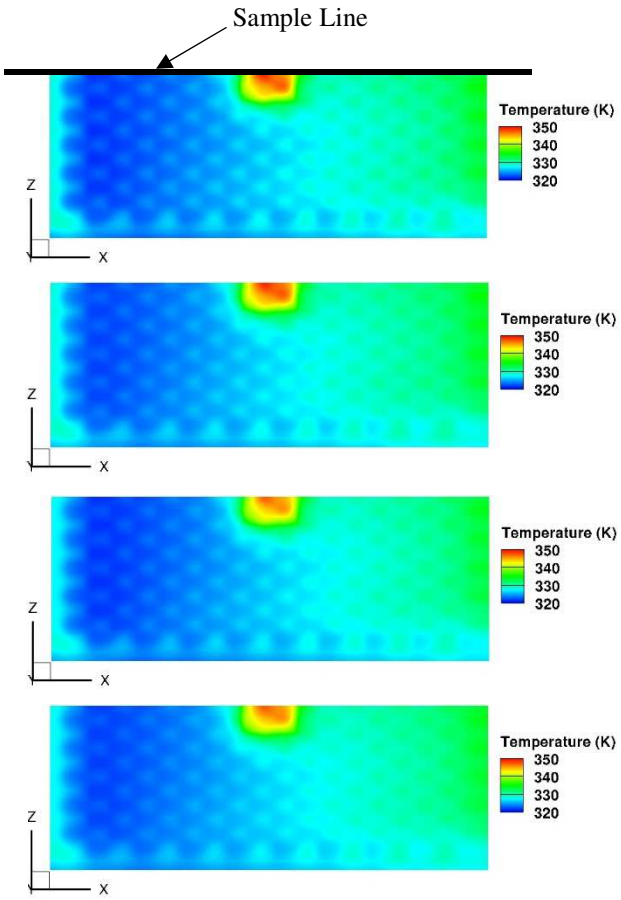

Figure 2. Temperature distribution on the top surface when using thermal conductivities for silicon for heat spreader thicknesses: a) 10 µm, b) 15 µm, c) 20 µm and d) 25 µm.

Figure 3 shows the temperature distribution along the sample line shown in Fig. 2. It should be noted that the oscillations in the temperatures coincide with the locations of the pin-fins directly below the hot surface. It can be seen that increasing the silicon thickness resulted in only 1 K decrease in maximum temperature.

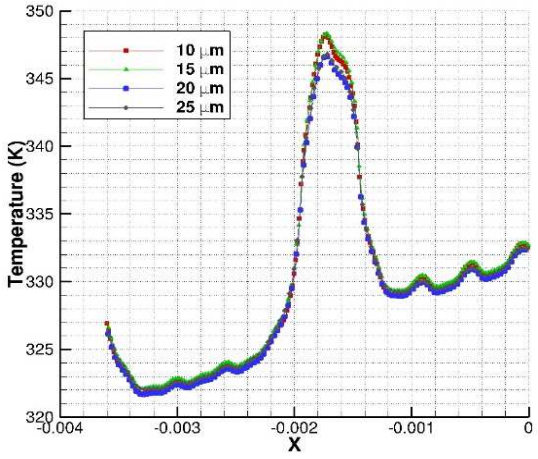

Figure 3. Temperature distribution along the sample line (Fig. 2a) for an entirely Silicon substrate.

ANALYSIS OF GRAPHENE HEAT SPREADERS

This study investigates the effect of not only GNP thin film thickness, but also the orientation of the platelets on the maximum temperature and temperature uniformity.

A total of five cases were considered and investigated using the 3D conjugate heat transfer analysis. The anisotropic thermal conductivity of GNP thin films is heavily dependent on several parameters. They can include temperature dependency, film thickness and orientation of the platelets, to name a few.

The thermal conductivities considered are given in Table 4. Cases A and D feature anisotropic thermal conductivities while cases B and C feature isotropic thermal conductivities. Cases A and C use properties of a single-layer graphene nano-platelets (SLGNP), while cases B and D use the properties of a few-layer graphene nano-platelets (FLGNP)

Table 4. In-plane and through-plane thermal conductivities of GNP based thin film heat spreaders analyzed

	In-Plane ($W\ m^{-1}K^{-1}$)	**Through-Plane ($W\ m^{-1}K^{-1}$)**
Case A [12]	5000	6
Case B	2000	2000
Case C	5000	5000
Case D [17]	500	3
Case E	3	500

Case A: Thin Coating with Single Layer GNPs

The directional conductivities heavily depend on the orientation of the platelets. Figure 4 shows the preferential in-plane orientation. The thermal conductivity of GNP, as reported by some manufacturers [18], is 3000 W m^{-1} K^{-1} in-plane and 6 W m^{-1} K^{-1} through-plane. Others have also stated that the in-plane conductivity can reach as high as 5000 W m^{-1} K^{-1} [18]. These values of conductivity are valid only for thin films of single to a few atomic layers. These thermal conductivities were used for micron-levels of thickness for curiosity's sake.

This section investigates the effect of these levels of conductivities. The platelets were assumed to be oriented so that the in-plane conductivity is in the "x-z" plane and the through-plane conductivity in the "y" direction (see Fig. 1).

Many works on GNP thin films in the past have neglected the effects of contact resistance. Chen *et al.* [19] investigated the contact conductance of graphene on silicon dioxide. It was found that the contact resistance was on the order of 10^{-8} and ranged from 5.6 x 10^{-9} to 1.2 x 10^{-8} m^2 K W^{-1}. It was slightly lower than the experimental results reported by Yu *et al.* [20] indicating that thermal contact resistance is 9 x 10^{-8} m^2 K W^{-1}.

Table 5 shows the maximum temperature and coefficient of variation for the different thicknesses for Case A. It can be seen that here increasing the thickness drastically increases the maximum temperature, while the CV decreases.

Figure 4. Case A: A sketch of in-plane orientation of GNPs in thin films resulting in high in-plane thermal conductivity.

Figure 5 shows the temperature distribution on the top surface. It can be qualitatively seen that the temperature distribution is unaltered from thickness to thickness.

Table 5. Case A: Maximum temperature and CV for thermal conductivity for in-plane GNPs thin films.

t (μm)	Max. Temp. (K)	$CV_{Hotspot}$	$CV_{Background}$	ΔT_{avg}
10	357.90	0.00535	0.00815	14.672
15	366.07	0.00459	0.00753	15.731
20	374.51	0.00399	0.00700	16.883
25	382.93	0.00349	0.00642	18.084

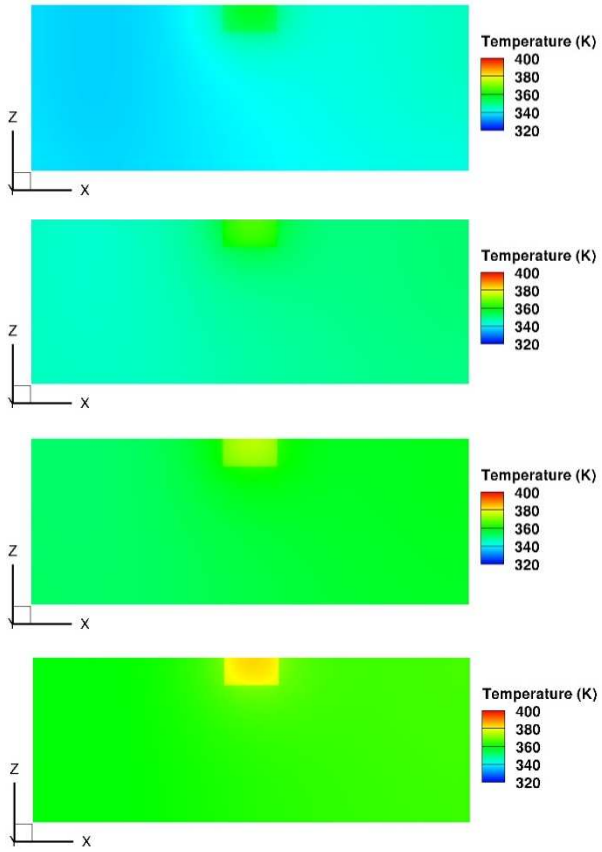

Figure 5. Case A: Temperature distribution on the top surface when using thermal conductivities for the GNP film thicknesses: a) 10 μm, b) 15 μm, c) 20 μm and d) 25 μm.

The temperature distribution along the sample line, shown in Fig. 6 and Table 5 indicates that with each addition of 5μm of thin film GNPs in Case A, the temperature increases by approximately 9°C which is highly undesirable.

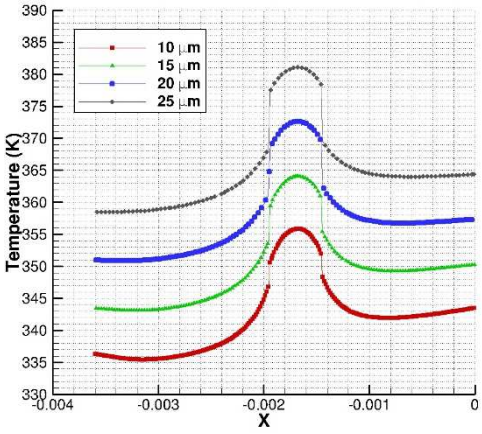

Figure 6. Case A: Temperature distribution along the sample line.

It can also be seen from Fig. 6 that everywhere along the sample line the temperature in Case A is elevated by the same amount. Temperature oscillations in the case without thin GNP films (Fig. 3) are no longer present suggesting that the preferentially in-plane orientation of GNPs improve local temperature uniformity, but not overall temperature uniformity.

Case B: Thin Coating with Isotropic GNPs

Although, GNP thin films exhibit high thermal conductivity, this high value of thermal conductivity is only experienced for a single "sheet" or atomic plane of GNP with an approximate thickness of 1 nm. Balandin [18] reported that the thermal conductivity drastically decreases with additional layers of GNP. It was stated that for a thin film consisting of more than four atomic layers, the thermal conductivity drops below that of the high quality bulk graphite, but with sufficient number of layers it recovers. Due to the sufficiently thick layers of GNP used in this work, it can be assumed that the thermal conductivity of GNP recovers to values of high quality bulk graphite ($k = 2000$ W m^{-1} K^{-1}) [18]. A thermal conductivity value of $k = 5000$ W m^{-1} K^{-1} was also investigated. The thermal conductivity of GNP film in this section was assumed to be isotropic, because of the random orientation of the GNPs, (Fig. 7) arising when creating films of large thicknesses [21]. The contact resistance value from the previous sections is also used here.

Figure 7. Case B: A sketch of random orientations of GNPs in thin films resulting in an isotropic thermal conductivity.

Table 6 shows the maximum temperatures and CV for Case B, with an isotropic thermal conductivity of 2000 W m^{-1} K^{-1}. Here, it can be seen that both the maximum temperature and CV decrease with increasing film thickness. It can also be seen that

the temperature difference between subsequent thicknesses decreases suggesting there exists an optimum thin film thickness beyond which the temperature will not decrease, but will instead begin to increase. This was confirmed in the excellent work by Fukutani and Shakouri [2].

Table 6. Case B: Maximum temperature and CV for thermal conductivity for isotropic GNP thin films.

t (μm)	Max. Temp. (K)	$CV_{Hotspot}$	$CV_{Background}$	ΔT_{avg}
10	338.31	0.0055	0.0089	9.266
15	336.42	0.0045	0.0086	7.886
20	333.97	0.0038	0.0085	6.692
25	333.00	0.0033	0.0083	6.008

Figure 8 shows the temperature on the top surface of IC in Case B. It can be seen that the heat is being dissipated away from the hot spot with increasing thickness of isotropic GNP based thin film heat spreaders.

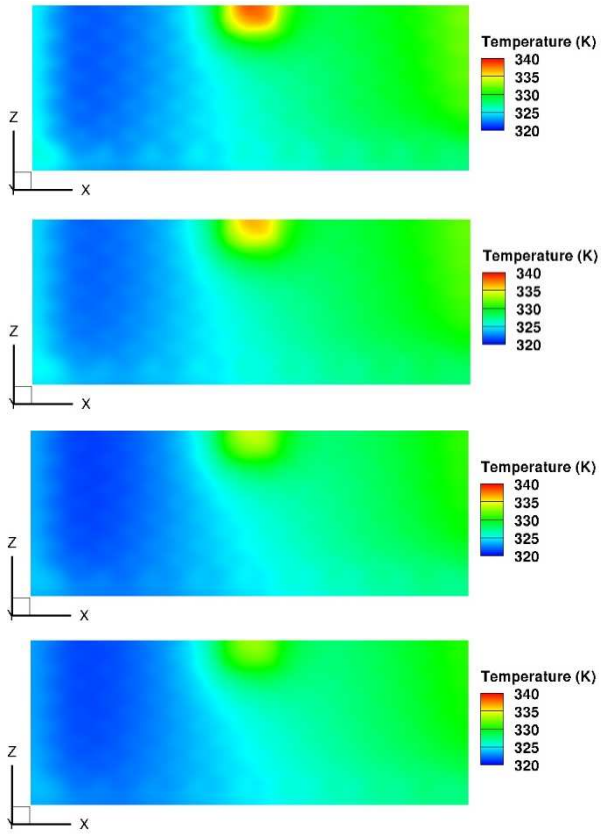

Figure 8. Case B: Temperature distribution on the top surface when using thermal conductivities for isotropic GNP film thicknesses: a) 10 μm, b) 15 μm, c) 20 μm and d) 25 μm.

Figure 9 shows the temperature distribution along the sample line for case B. It can be seen that the isotropic GNP thin film suppressed the local oscillations thereby increasing local temperature uniformity.

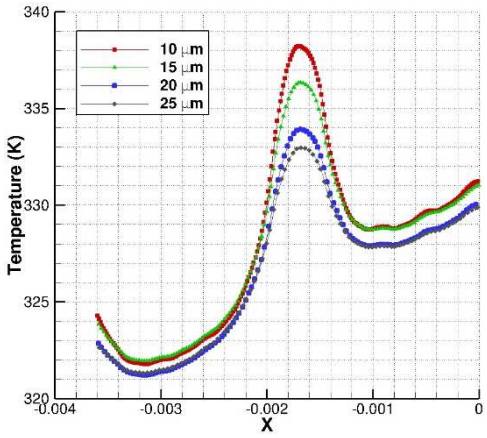

Figure 9. Case B: Temperature distribution along the sample line using isotropic GNP thin films.

It can also be seen that the maximum temperature is reduced and that temperature distribution is different for each thickness unlike when Single-Layer Graphene is used as in Case A.

Case C: Thin Coating with Isotropic GNPs

Table 7 shows the maximum temperature and CV for Case C. It can be seen that temperatures and CV are lower than those for Case B. This is due to the higher thermal conductivity.

Table 7. Case C: Maximum temperature and CV for high thermal conductivity isotropic GNP thin films.

t (μm)	Max. Temp. (K)	$CV_{Hotspot}$	$CV_{Background}$	ΔT_{avg}
10	334.03	0.00338	0.00835	6.140
15	332.41	0.00266	0.00795	4.887
20	330.42	0.00224	0.00776	4.003
25	329.70	0.00197	0.00748	3.463

Figure 10 shows the temperature distribution on the top surface for Case C. It can be seen from the higher upstream temperature that the heat is conducted further upstream.

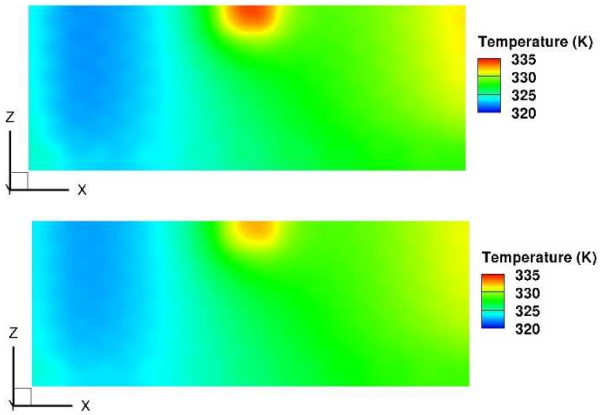

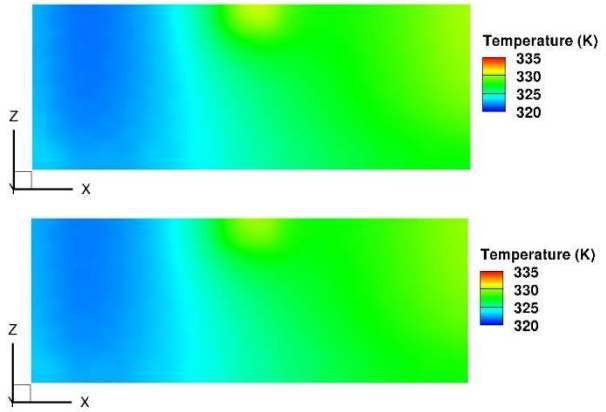

Figure 10. Case C: Temperature distribution on the top surface when using thermal conductivities for isotropic GNP film thicknesses: a) 10 µm, b) 15 µm, c) 20 µm and d) 25 µm.

Case D: Thin Coating with Few-Layer GNPs

Certain manufacturers [17] are also able to produce sufficiently thick graphene films, while maintaining the anisotropic behavior. They reported, for thickness as the ones considered in this work, that thick GNP films have an in-plane thermal conductivity of 500 W m^{-1} K^{-1} and a through-plane conductivity of 3 W m^{-1} K^{-1}. The GNPs are assumed to be oriented such that the in-plane conductivity is in the "x-z" plane and the through-plane conductivity in the "y" direction. The value of contact resistance from previous sections was used in this analysis.

Table 8 shows the maximum temperature and CV for Case D. It can be seen that increasing the thickness drastically increases both the maximum temperature and CV as it did in the case with Single-Layer Graphene (Case A).

Table 8. Case D: Maximum temperature and CV for thermal conductivity having in-plane GNPs.

t (µm)	Max. Temp. (K)	$CV_{Hotspot}$	$CV_{Background}$	ΔT_{avg}
10	406.91	0.01751	0.00982	41.964
15	430.82	0.01802	0.01039	49.700
20	452.10	0.01740	0.01100	55.593
25	471.64	0.01633	0.01141	60.304

Figure 11 shows the temperature distribution on the top surface. As in Case A, it can again be seen that the distribution shape is unaffected by the film thickness, but the magnitude is affected.

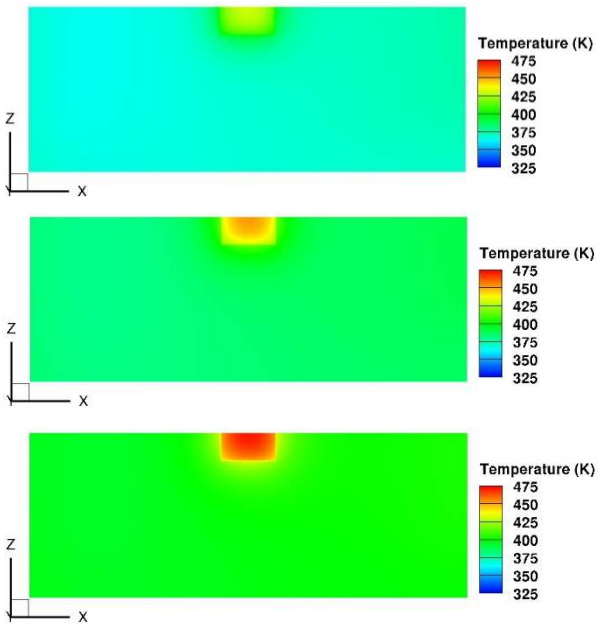

Figure 11. Case D: Temperature distribution on the top surface when using thermal conductivities for the GNP film thicknesses: a) 10 µm, b) 15 µm, c) 20 µm and d) 25 µm.

Figure 12 shows the distribution along the sample line. It can be seen that the temperature increases by approximately 20°C for each additional five microns in film thickness.

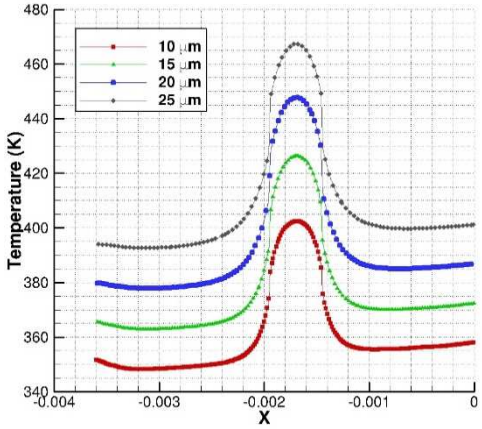

Figure 12. Case D: Temperature distribution along the sample line having thin films with in-plane GNPs.

In Case A and Case D, the GNP orientation was such that the thermal energy in the thin film was dissipated towards side walls that were thermally insulated. With such poor through-plane thermal conductivity, the heat cannot be conducted towards and into the fluid channel, the only means by which it can be removed.

Case E: Thin Coating with Through-Plane GNPs

For this reason, Tian *et al.* [21] suggested an alternative orientation of the GNPs. Thin films with a preferential through-plane orientation (Fig. 13) of the GNPs were also investigated as Case E. Here, GNPs were assumed to be oriented such that the in-plane conductivity is in the "x-y" plane and the through-

plane conductivity in the "z" direction (Fig. 1). That is, in Case E, GNPs were oriented in the x-y plane (perpendicular to z-axis) so that the energy is diffused down into the channel and in the streamwise direction. The z-direction (cross-stream direction) will have a lower thermal conductivity.

Table 9 shows the maximum temperature and CV for GNP orientation shown in Fig. 13. It can be seen that the temperature is lower than in the case without thin films. The CVs, however, differ insignificantly.

Figure13. Case E: A sketch of orientation of GNPs in thin films resulting in high through-plane thermal conductivity.

Table 9. Case E: Maximum temperature and CV for thermal conductivity for preferential through-plane orientation.

t (μm)	Max. Temp. (K)	$CV_{Hotspot}$	$CV_{Background}$	ΔT_{avg}
10	344.88	0.00889	0.00945	14.060
15	343.99	0.00843	0.00929	13.580
20	343.45	0.00807	0.00926	13.264
25	342.88	0.00768	0.00914	12.985

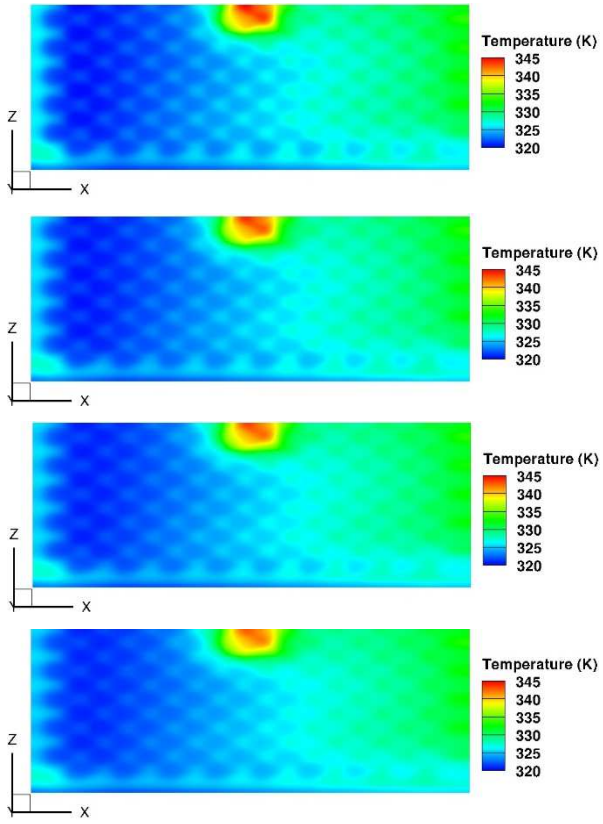

Figure 14. Case E: Temperature distribution on the top surface when using thermal conductivities for preferential through-plane orientation for GNP film thicknesses: a) 10 μm, b) 15 μm, c) 20 μm and d) 25 μm.

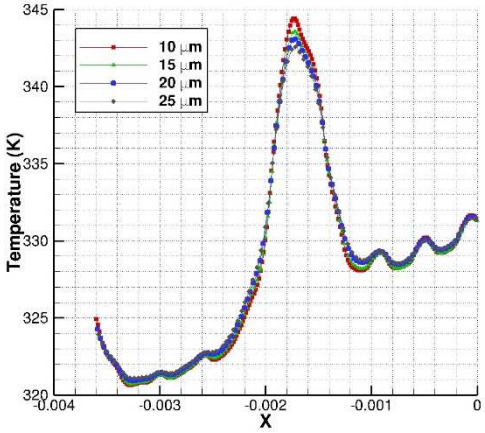

Figure 15. Case E: Temperature distribution along the sample line for preferential through-plane orientation of the GNPs in the films.

Figure 14 shows the temperature distribution on the top surface of the chip. The cooler temperatures away from the hot spot, in the cross-stream direction, suggest that heat is being conducted more in the stream-wise direction and into array of micro pin-fins. This is expected due to the orientation of the GNPs.

Figure 15 shows the temperature along the sample line for preferential through-plane orientation. It can be seen, from the temperature oscillations, that this orientation does not improve local temperature uniformity. The preferential in-plane orientation of GNPs is able to improve local uniformity, but not overall temperature uniformity. The isotropic thin films are better able to dissipate heat in all directions.

CONCLUSIONS

The effects of graphene nano-platelets (GNP) thin films heat spreaders on a hot surface of an integrated circuit (IC) electronic chip internally convectively cooled via forced convection through an array of micro pin-fins, have been investigated computationally using 3D conjugate heat transfer analysis. These thin film heat spreaders were applied to an optimized micro pin-fin array configuration featuring a hot spot. The objective was to elucidate the effect of non-isotropic and isotropic GNP based thin film heat spreaders on the maximum temperature at a hot spot and temperature uniformity of the hot surface. The effect of thin film thickness, graphene thermal conductivity and orientation of the nano-platelets were investigated. was shown that the platelets must be oriented in such a way that the maximum directional thermal conductivity is in the direction where there is a greater capability of heat removal.

The thin films were found to increase maximum temperature and temperature uniformity when the platelets were oriented parallel to the hot surface. When orienting them orthogonal to the hot surface (towards the fluid cooling channel), the maximum temperature decreased below that of the

configuration without thin film. It was also found that for this array of pin-fins, the preferentially in-plane orientation was able to increase local temperature uniformity, but not overall uniformity.

The isotropic thin films were able to significantly lower maximum temperature, while increasing both local and overall temperature uniformity. For isotropic films, it was confirmed that an optimum film thickness exists, beyond which the decrease in temperature is negligible.

It was confirmed that a proper thin film thickness, which affects thermal conductivity, and a proper platelet orientation can lead to a significant reduction in maximum temperature.

ACKNOWLEDGEMENTS

The lead author gratefully acknowledges the financial support from Florida International University in the form of an FIU Presidential Fellowship. The authors are grateful for the partial financial support of this research provided by DARPA grant HR0011-14-1-0002 via GaTech grant RE314-G1 in the framework of ICECool project under supervision of Dr. Avram Bar-Cohen. The views and conclusions contained herein are those of the authors and should not be interpreted as necessarily representing the official policies or endorsements, either expressed or implied, of DARPA or the U.S. Government.

REFERENCS

[1] A. Bar-Cohen, "Gen-3 Thermal Management Technology: Role of Microchannels and Nanostructures in an Embedded Cooling Paradigm," *Journal of Nanotechnology in Engineering and Medicine*, Vol. 4, 020907, 2013.

[2] K. Fukutani and A. Shakouri, "Optimization of Thin Film Microcoolers for Hot Spot Removal in Packaged Integrated Circuit Chips," *22nd IEEE SEMI-THERM Symposium*, March 14-16, Dallas, Texas, pp. 130-134, 2006.

[3] P. Wang, P. McCluskey and A. Bar-Cohen, "Hybrid Solid- and Liquid-Cooling Solution for Isothermalization of Insulated Gate Bipolar Transistor Power Electronic Devices." *IEEE Transactions on Components, Packaging and Manufacturing Technology*, Vol. 3, pp. 601-611, 2013.

[4] P.M. Mayer and R.J. Ram, "Optimization of Heat Sink-Limited Thermoelectric Generators," *Nanoscale and Microscale Thermophysical Engineering*, Vol. 10, pp. 143-155, 2006.

[5] M. Smalc, G. Shives, G. Chen, S. Guggari and J. Norley, "Thermal Performance of Natural Graphite Heat Spreaders," *Interpack2005-73073*, July 17-22, San Francisco, California, 2005.

[6] S. R. Reddy, A. Abdoli, G.S. Dulikravich and R. Jha, "Conjugate Analysis of Thin Film Heat Spreaders to Reduce Temperature at Hot Spots," *IMECE2015-52804*, Nov. 13-19, Houston, Texas, USA, 2015.

[7] A. Barua, Md.S. Hossain, K.I. Massod and S. Subrina, "Thermal Management in 3-D Integrated Circuits with Graphene Heat Spreaders," *Physics Procedia*, Vol. 25, pp. 311-316, 2012.

[8] S.H. Bae, R. Shabani, J.B. Lee and S.J. Baeck, "Graphene-Based Heat Spreader on Flexible Electronic Devices," *IEEE Transactions on Electron Devices*, Vol. 26, pp. 4171-4175, 2014.

[9] A. Subrina, D. Kotchethov, A.A. Balandin, "Heat Removal in Silicon-on-Insulator Integrated Circuits With Graphene Lateral Heat Spreaders," *IEEE Electron Device Letters*, Vol. 30, pp. 1281-1283, 2009.

[10] S.R. Reddy, A. Abdoli, G.S. Dulikravich, C. Pacheco, G. Vasquez, R. Jha, M.J. Colaco, H.R.B. Orlande, "Multi-Objective Optimization of Micro Pin-Fin Arrays for Cooling of High Heat Flux Electronic Devices With a Hot Spot", *Heat Transfer Engineering*, Vol. 38, 2017.

[11] S.R. Reddy and G.S. Dulikravich, 2015, "Inverse Design of Cooling of Electronic Chips Subject to Specified Hot Spot Temperature and Coolant Inlet Temperature," *Heat Transfer Engineering*, Vol. 38, 2017.

[12] A. A. Balandin, S. Ghosh, W. Bao, I. Calizo, D. Teweldebrhan, F. Miao, C. N. Lau, "Superior Thermal Conductivity of Single-Layer Graphene," *Nano Letters*, Vol. 8, pp. 902-907, March 2008.

[13] S. Ghosh, I. Calizo, D. Teweldebrhan, E. P. Pokatilov, D. L. Nika, A. A. Balandin, W. Bao, F. Miao, and C. N. Lau, "Extremely High Thermal Conductivity of Graphene: Prospects for Thermal Management Applications in Nanoelectronics," *Applied Physics Letters*, Vol. 92, p. 151911, April 2008.

[14] D.L. Nika, E.P. Pokatilov, A.S. Askerov and A.A. Balandin, "Phonon Thermal Conduction in Graphene: Role of Umklapp and Edge Roughness Scattering," *Phys. Rev. B,* Vol. 79, p. 155413, April 2009.

[15] S. Ghalambor, "Analytical Solution of Steady-State Heat Conduction in Multi-Layer Stack Packaging," *Ph.D. Dissertation,* University of Texas at Arlington, 2014.

[16] F. Alfieri, M.K. Tiwari, A. Renfer, T. Brunschwiler, B. Michel, D. Poulikakos, "Computational Modeling of Vortex Shedding in Water Cooling of 3D Integrated Electronics", *International Journal of Heat and Fluid Flow*, Vol. 44, pp. 745-755, Dec. 2013.

[17] STREAM Graphene Nanoplatelets, www.stream.com, visited September 2016.

[18] A.A. Balandin, "Thermal Properties of Graphene and Nanostructured Carbon Materials", *Nature Materials*, Vol. 10, pp. 569-581, 2011.

[19] Z. Chen, W. Jang, W. Bao, C.N. Lau and C. Dames, Thermal Contact Resistance Between Graphene and Silicon Dioxide, *Applied Physics Letters*, Vol. 95, 2009

[20] C. Yu, S. Saha, J. Zhou, L. Shi, A.M. Cassell, B.A. Cruden, Q. Ngo and J. Li, "Thermal Contact Resistance and Thermal Conductivity of a Carbon Nanofiber", *ASME Journal of Heat Transfer,* Vol. 128, pp. 234-239, 2006.

[21] X. Tian, M.E. Itkis, E.B. Bekyarova and R.C. Haddon, "Anisotropic Thermal and Electrical Properties of Thin Thermal Interface Layers of Graphite Nanoplatelet-Based Composites," *Nature Scientific Reports*, pp. 1-6, 2013.